Available online at www.sciencedirect.com
SCIENCE DIRECT®
Journal of Nuclear Materials 328 (2004) 151–164
journal of nuclear materials
www.elsevier.com/locate/jnucmat

INCAS: an analytical model to describe displacement cascades

Stéphanie Jumel [a,b,*], Jean Claude Van-Duysen [a,b]

[a] EDF/R&D site des Renardières, Route des Renardières, F-77818 Moret sur Loing, France
[b] Laboratoire de Métallurgie Physique et Génie des Matériaux, UMR 8517, Bât. C6, Université de Lille I, F-59655 Villeneuve d'Ascq cedex, France

Received 22 July 2003; accepted 18 March 2004

Abstract

REVE (REactor for Virtual Experiments) is an international project aimed at developing tools to simulate neutron irradiation effects in Light Water Reactor materials (Fe, Ni or Zr-based alloys). One of the important steps of the project is to characterise the displacement cascades induced by neutrons. Accordingly, the Department of Material Studies of Electricité de France developed an analytical model based on the binary collision approximation. This model, called INCAS (INtegration of CAScades), was devised to be applied on pure elements; however, it can also be used on diluted alloys (reactor pressure vessel steels, etc.) or alloys composed of atoms with close atomic numbers (stainless steels, etc.). INCAS describes displacement cascades by taking into account the nuclear collisions and electronic interactions undergone by the moving atoms. In particular, it enables to determine the mean number of sub-cascades induced by a PKA (depending on its energy) as well as the mean energy dissipated in each of them. The experimental validation of INCAS requires a large effort and could not be carried out in the framework of the study. However, it was verified that INCAS results are in conformity with those obtained from other approaches. As a first application, INCAS was applied to determine the sub-cascade spectrum induced in iron by the neutron spectrum corresponding to the central channel of the High Flux Irradiation Reactor of Oak Ridge National Laboratory.

1. Introduction

REVE (REactor for Virtual Experiments) is an international project (e.g., [1,2]) aimed at developing tools to simulate neutron irradiation effects in Light Water Reactor (LWR) materials (Fe, Ni or Zr-based alloys). One of the important steps of the project is to describe the displacement cascades induced by neutrons. The required information is essentially the number of sub-cascades, the dissipated energy in each sub-cascade and the number of Frenkel pairs produced between the sub-cascades. Several simulation codes based on Binary Collision Approximation (e.g., Marlowe [3], Trim [4]) can already provide this information. However, using them presents some difficulties for the aimed application, e.g.,

- the identification of sub-cascades is not straightforward. It requires the analysis of the shape and size of the zones where point defects are produced [5] or the measurement of the local density of vacancies [6]. Such post-treatments are rather complex.
- it is necessary to carry out a large number of simulations to get statistically-relevant information.

To get round these difficulties, the Department of Materials Studies of Electricité de France developed an analytical model based on the binary collision approximation. This model, called INCAS (INtegration of CAScades), relies on a simple definition of the

* Corresponding author. Tel.: +33-6 14 40 01 21.
E-mail addresses: stephanie.jumel@edf.fr (S. Jumel), jean-claude.van-duysen@edf.fr (J.C. Van-Duysen).

0022-3115/$ - see front matter © 2004 Elsevier B.V. All rights reserved.
doi:10.1016/j.jnucmat.2004.03.012

sub-cascades and directly leads to average results. It was set up to be used on pure elements; however, it can be also applied to diluted alloys (reactor pressure vessel steels, etc.) or alloys mainly composed of atoms with close atomic number (stainless steels, etc.).

The objective of the present article is to describe the proposed model and some of its results. Most of the used equations are classical and very well known by the 'Binary Collision' community. However, for INCAS to be easily usable by teams working on irradiation effects in LWR materials, these equations are explicitly derived in the article. Section 2 reviews some elements about the displacement cascade phenomenon. In Section 3, we present the proposed model and the corresponding equations. Section 4 is dedicated to the determination of the required characteristics of displacement cascades. Finally, in Section 5, INCAS is applied to some examples and compared to other methods.

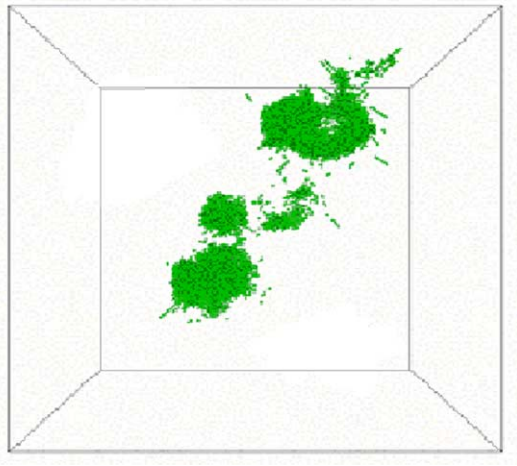

Fig. 1. Displacement cascade simulated in iron by Molecular Dynamics; the cascade splits into two or three sub-cascades. $E_{PKA} = 40$ keV, $T = 100$ K [10].

2. Displacement cascades

In materials under neutron irradiation, neutrons may collide with lattice-atoms which are called Primary Knock-on Atoms (PKAs). If the transferred energy during such a collision is higher than the displacement threshold energy E_d (e.g., for iron, E_d has an effective value of 40 eV [7]), the PKA leaves its site and starts moving [1,2] through the lattice. During its displacement, a PKA may be slowed-down by interactions with electrons and/or collisions with other atoms, which are called Secondary Knock-on Atoms (SKAs) (e.g., [8]). These SKAs can also leave their site and then be slowed-down by the same mechanisms; the tertiary knock-on atoms can proceed the same way and so on. This leads to a series of atomic displacements, called a 'displacement cascade'. After all the PKA energy has been dissipated in such interactions, most of the created vacancies and self-interstitial atoms annihilate each other. At the end of this recombination phase, only some residual point defects remain. The overall event lasts only some picoseconds.

If the PKA energy is high enough (few tens of keV for metals (e.g., [9,10]), the cascade can split into sub-cascades (Fig. 1). As generally proposed (e.g., [5,6]), it can be considered that sub-cascades are formed whenever a large part of the atomic displacements occurs in well defined zones which do not overlap each others. Between the sub-cascades, the PKA also produces atomic displacements, but they are fewer and localized mainly along the PKA trajectory.

The slowing-down of moving atoms (PKAs, SKAs, etc.) is essentially controlled by electronic interactions in the high velocity range (e.g., $E > 1$ MeV for iron) and by atomic collisions in the low velocity range (e.g., $E < 150$ keV for iron) [11–13]. For the LWR-type neutron spectra, displaced atoms have a maximal kinetic energy of about 3 MeV. This energy is high enough for both types of slowing-down processes to be considered. For each moving atom we thus have to consider both an electronic $(dE/dx)_e$ and a nuclear $(dE/dx)_n$ stopping power; these two functions characterise the energy losses per unit length of displacement. The total stopping power is given by

$$(dE/dx)_{tot} = (dE/dx)_n + (dE/dx)_e. \quad (1)$$

After emerging from the recoil events, displaced atoms may be singly or multiply ionised. However, in any cases, they rapidly approach a charge equilibrium (e.g., a few lattice constants for iron atoms in the keV range) which can be estimated with good accuracy on the basis of the Bohr model [14]

$$q_{equi} = Z_1(1 - e^{-v/v_0 Z_1^{2/3}}), \quad (2)$$

where v and Z_1 are the velocity and the atomic number of the moving atom, v_0 is the Bohr velocity ($v_0 = 2.2 \times 10^6$m/s). For the considered kinetic energy ($E \leqslant 3$ MeV), q_{equi} is always very low and can be neglected in the quantification of $(dE/dx)_e$ and $(dE/dx)_n$.

[1] In this simplified description of neutron–atom interactions, inelastic interactions and in particular possible nuclear reactions [(n,p), (n,α), $(n,2n)$, etc.] are not accounted for.

[2] The moving atoms may be ions; their ionisation level increases with their velocity.

2.1. Electronic interactions

Since q_{equi} is negligible, it can be considered that the electronic interactions undergone by moving atoms mainly result from their collisions with the electrons of the other atoms (conduction electrons in the case of metals). Hence, the electronic stopping power can be expressed only by the Lindhard–Scharff expression [3] [12]

$$\left(\frac{\mathrm{d}E}{\mathrm{d}x}\right)_{\mathrm{e}} = NS_L(E) \quad \text{where } S_L(E) = kE^{1/2}, \tag{3}$$

with

$$k = \frac{8\pi e^2 a_0 Z_1^{7/6} Z_2}{(Z_1^{2/3} + Z_2^{2/3})^{3/4} M_1^{1/2} v_0} \ (\mathrm{eV}^{1/2}\,\mathrm{m}^2), \tag{4}$$

where Z_1 and Z_2 are, respectively, the atomic numbers of the moving and lattice-atoms, M_1 is the atomic mass of the moving atom, $a_0 = 5.3 \times 10^{-11}$ m is the Bohr radius, $v_0 = 2.2 \times 10^6$ m/s is the Bohr velocity, $e^2 = \frac{2.2 \times 10^6 h}{2\pi}$ eV m where h is the Planck constant $= 4.135 \times 10^{-15}$ eV s.

Fig. 2 shows the evolution of Lindhard–Scharff electronic stopping power versus the kinetic energy of an iron atom moving in iron.

2.2. Atomic collisions

Collisions between atoms can be treated in the framework of the binary collision approximation, i.e., they only concern two atoms at a time and do not depend on their environment. These collisions are also supposed to be elastic (the internal energy of each particle is the same before and after the collision) and not affected by the small equilibrium charge of moving atoms. Let us consider a collision between an incident atom and a target atom. The incident atom has a kinetic energy E before the collision and E' after the collision. During this collision, it transfers an elastic energy E-E' to the target atom. If this energy is:

- higher than the displacement threshold energy E_{d}, then the hit atom leaves permanently its site with a kinetic energy $T = E - E' - \varepsilon'$, where ε' is its binding energy; in this study we neglect ε' and consider $T = E - E'$ (thus the kinetic energy of the hit atom equals the transferred energy).
- lower than E_{d}, then the hit atom cannot leave its site.

[3] The Lindhard–Scharff expression can be used for PKA energies up to about 100 MeV. It is often attributed to Lindhard–Scharff–Schiot.

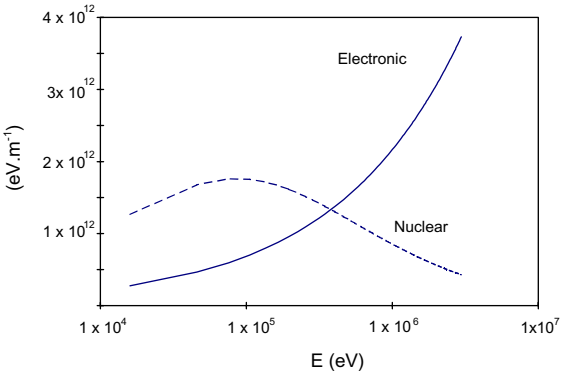

Fig. 2. Evolution of the nuclear and electronic stopping powers versus the kinetic energy of an iron atom moving in iron.

The description of the atomic interactions can be made with the following quantities, expressed as a function of the energy of the incident atom.

- *the differential cross section for collision between the incident and target atoms*: we use the expression proposed by Winterbon et al. [13] and derived from a Thomas–Fermi type potential. It is expressed as

$$\begin{aligned}\mathrm{d}\Sigma(E) &= \Sigma(E \to E')\mathrm{d}E' \\ &= \left(\frac{\pi a^2}{2t^{3/2}}\right)\frac{\lambda t^{1/2-m}\mathrm{d}t}{[1 + (2\lambda t^{1-m})^q]^{1/q}},\end{aligned} \tag{5}$$

where: $t = E(E - E')\frac{M_2}{M_1}\left(\frac{a}{2Z_1 Z_2 e^2}\right)^2$, $a = \frac{0.885 a_0}{(Z_1^{2/3} + Z_2^{2/3})^{1/2}}$ is the Lindhard screening radius, $a_0 = 5.3 \times 10^{-11}$ m is the Bohr radius, Z_1 and Z_2 are, respectively, the atomic numbers of the incident and target atoms, M_1 and M_2 are, respectively, the atomic masses of the incident and target atoms, $e^2 = \frac{2.2 \times 10^6 h}{2\pi}$ eV m where h is the Planck constant $= 4.135 \times 10^{-15}$ eV s.

Considering the PKA energy range used in this study ($E \leqslant 3$ MeV), we use the Winterbon's values [15] for the parameters of expression (5):

$$\lambda = 2.92 \quad m = 0.191 \quad q = 0.512$$

- *the total cross section for collisions with a transferred energy higher than x*

$$\Gamma_x(E) = \int_0^{E-x} \Sigma(E \to E')\mathrm{d}E', \tag{6}$$

- *the probability density for the incident atom to have a kinetic energy E′ after a collision with a transferred energy higher than x*

$$\Pi_x(E \to E') = \frac{\Sigma(E \to E')}{\Gamma_x(E)}, \tag{7}$$

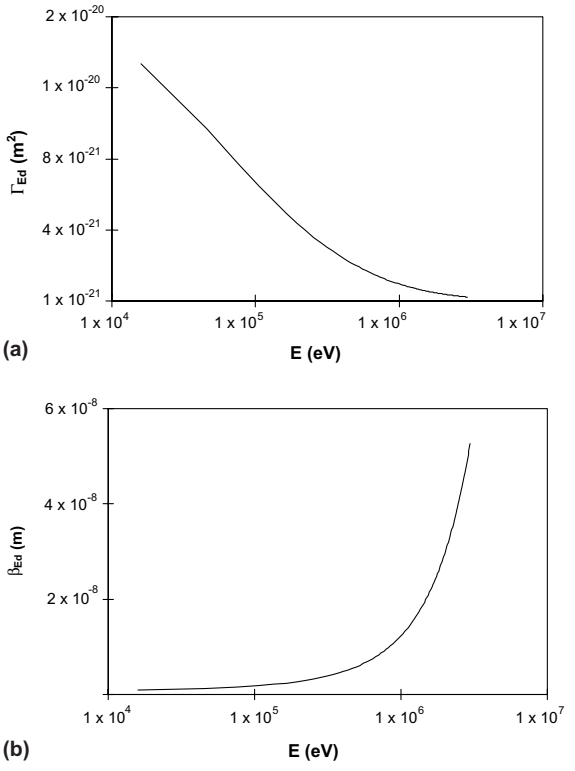

Fig. 3. Evolution of $\Gamma_{E_d}(E)$ and $\beta_{E_d}(E)$ versus the kinetic energy E of an iron atom moving in iron ($E_d = 40$ eV).

- *the mean distance between two such collisions*

$$\beta_x(E) = \frac{1}{N\Gamma_x(E)}, \tag{8}$$

where N is the atomic density of the target material. As an example, $\Gamma_{E_d}(E)$ and $\beta_{E_d}(E)$ obtained by setting $x = E_d = 40$ eV in (6) and (8), are presented in Fig. 3 for an iron atom moving in iron.

- *Nuclear stopping power*

$$\left(\frac{dE}{dx}\right)_n = N\int_0^E \Sigma(E \to E')[E - E']dE'. \tag{9}$$

Fig. 2 shows the evolution of the nuclear stopping power versus the kinetic energy of an iron atom moving in iron.

3. Presentation of the proposed model

In order to characterise the displacement cascade induced by a PKA, the simplest approach consists in following the latter until it stops and describing its interactions with the matter along its trajectory (atomic collisions and electronic interactions). However, after a nuclear collision, the SKA may be more energetic than the PKA and hence induce most of the subsequent damage. To give a better description of a displacement cascade, after each atomic collision, it is therefore preferable to follow the fate of the atom with the highest energy. To establish the required formalism, let us consider a PKA with an energy E just before a nuclear collision; after the collision we call [16]:

- PKA, the atom with the highest kinetic energy, noted E',
- SKA, the atom with the lowest kinetic energy, noted $T = E - E'$.

The two possible configurations that can happen during a collision are illustrated in Fig. 4. For each of them, $E' \geqslant T$, which leads to $E' \geqslant E/2$ and $T \leqslant E/2$; these inequalities will be considered to define the limits of some integrals used in the model. With such conventions, the PKA moving in the material is not a single atom but a series of atoms. Along its trajectory, it successively corresponds to the atoms which leave the collision sites with the highest energy, i.e., the PKA can be the same atom before and after the collision (case a in Fig. 4) or can be swapped with the lattice-atom (case b in Fig. 4). The equations that can be deduced from these conventions are presented hereafter.

- *Cross section*: we can define the total cross section for collisions in which the SKA has a kinetic energy higher than a given value x

$$\begin{aligned}\Sigma_x(E) &= \int_{E/2}^{E-x} \Sigma(E \to E')dE' + \int_x^{E/2} \Sigma(E \to T)dT \\ &= \int_x^{E-x} \Sigma(E \to E')dE'. \end{aligned} \tag{10}$$

The first and second integrals of the central part of (10) describe, respectively, the cases a and b of Fig. 4.

- *Probability densities of collisions:* considering only the collisions for which the SKA has a kinetic energy higher than x, the probability density for the PKA to have a kinetic energy E' after the collision is

$$P_x(E \to E') = \frac{\Sigma(E \to E')}{\Sigma_x(E)} + \frac{\Sigma(E \to E - E')}{\Sigma_x(E)}, \tag{11}$$

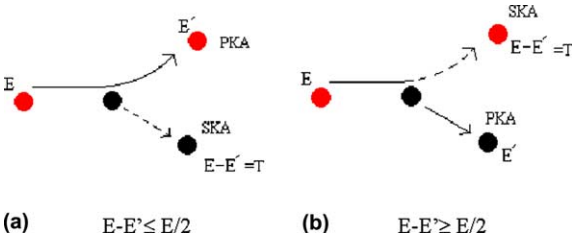

Fig. 4. Collision conventions where: (a) the incident atom remains the PKA after the collision, (b) the target becomes the PKA after the collision.

which may be written as a function of the variable T to express the probability density for the SKA to have a kinetic energy T after the collision

$$P_x(E,T) = P_x(E \to E') = \frac{\Sigma(E \to E-T)}{\Sigma_x(E)} + \frac{\Sigma(E \to T)}{\Sigma_x(E)}. \quad (12)$$

Several values of x will be considered in the following paragraphs.

- *Nuclear stopping power:* the nuclear stopping power of the PKA is given by

$$\left(\frac{dE}{dx}\right)_n = N\int_{E/2}^{E}(E-E')[\Sigma(E\to E')+\Sigma(E\to E-E')]dE'. \quad (13)$$

- *Electronic stopping power:* as previously mentioned, within the kinetic energy range taken into account in REVE, only the Lindhard–Scharff's contribution is relevant for the description of the electronic stopping powers of moving atoms. The corresponding expression is not modified by the proposed conventions

$$\left(\frac{dE}{dx}\right)_e = NkE^{1/2}, \quad (14)$$

with k given by (4).

3.1. Size of damage zones

We consider that a nuclear collision induces damages only if it creates at least one stable Frenkel pair (the transferred energy thus has to be higher than E_d). For such collisions, we call 'damage zone' the volume affected by the slowing-down of the SKA and we characterise this volume by its spherical envelop (Fig. 5). The sphere's diameter is given by the penetration depth of the SKA.

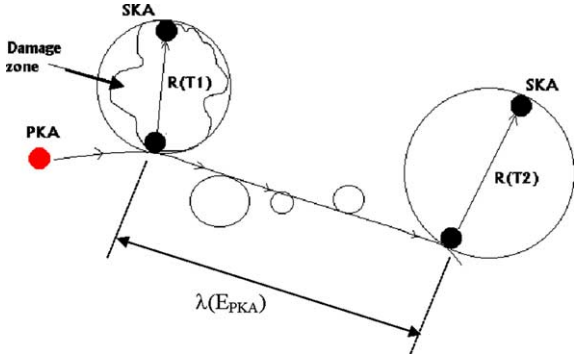

Fig. 5. Two 'high transferred energy' damage zones ($T1$ and $T2 \geqslant a_{sub}$) separated by three 'low transferred energy' damage zones. The 'high transferred energy' damage zones are considered as being sub-cascades.

- *Penetration depth of a SKA*: during its slowing-down, a SKA with an initial kinetic energy T_0 covers a distance $R(T_0) = \int_0^{T_0} \frac{dT}{(dT/dx)_{tot}}$. According to Sigmund [17], the penetration depth $R_P(T_0)$ is given by

$$R_P(T_0) = 0.73R(T_0) = 0.73\int_0^{T_0}\frac{dT}{(dT/dx)_{tot}}. \quad (15)$$

- *Mean size of a damage zone:* the mean size of the damage zone created during a collision with a transferred energy higher than E_d is obtained by averaging the possible SKA penetration depths

$$R_{E_d}(E) = \int_{E_d}^{E/2} R_P(T)P_{E_d}(E,T)dT, \quad (16)$$

where $P_{Ed}(E,T)$ is obtained by setting $x = E_d$ in equation (12).

3.2. Sub-cascades

We consider that damage zones are sub-cascades if they fulfil the two following criteria (Fig. 5):

- the dissipated energy in each of these zones is higher than a threshold value 'a' ($T_0 \geqslant a$) [17]. We call 'high transferred energy' damage zones, the damage zones respecting this criteria and 'low transferred energy' damage zones the other ones. At first sight the value of 'a' depends on the irradiated element;
- they do not overlap each other.

(a) 'high transferred energy' damage zones

By setting $x = a$ in Eqs. (10)–(12), we define the following equations.

- *the total cross section for collisions* inducing the formation of 'high transferred energy' damage zones ($T_0 \geqslant a$) is given by

$$\Sigma_a(E) = \int_a^{E-a}[\Sigma(E\to E')]dE', \quad (17)$$

- *the probability density for the PKA* to have an energy E' after such a collision

$$P_a(E\to E') = \frac{\Sigma(E\to E')}{\Sigma_a(E)} + \frac{\Sigma(E\to E-E')}{\Sigma_a(E)}, \quad (18)$$

- *the probability density for the SKA* to have an energy T after such a collision

$$P_a(E,T) = P_a(E\to E') = \frac{\Sigma(E\to E-T)}{\Sigma_a(E)} + \frac{\Sigma(E\to T)}{\Sigma_a(E)}, \quad (19)$$

- *the mean size* of a 'high transferred energy' damage zone

$$R_a(E) = \int_a^{E/2} R_P(T)P_a(E,T)dT, \quad (20)$$

- *the mean distance between two successive collisions* inducing 'high transferred energy' damage zones

$$\lambda_a(E) = \frac{1}{N\Sigma_a(E)}. \tag{21}$$

(b) 'Low transferred energy' damage zones

By analogy with the precedent paragraph, we define:

- *the total cross section for collisions* inducing the formation of 'low transferred energy' damage zones ($E_d \leqslant T_0 < a$)

$$\Sigma_{<a}(E) = \int_{E-a}^{E-E_d} \Sigma(E \to E')\mathrm{d}E' + \int_{E_d}^{a} \Sigma(E \to T)\mathrm{d}T. \tag{22}$$

The two integrals in (22), respectively, correspond to cases *a* and *b* of Fig. 4.

- *the probability density for the PKA* to have an energy E' after such a collision

$$P_{<a}(E \to E') = \frac{\Sigma(E \to E')}{\Sigma_{<a}(E)} + \frac{\Sigma(E \to E - E')}{\Sigma_{<a}(E)}, \tag{23}$$

- *the probability density for the SKA* to have an energy T after such a collision

$$P_{<a}(E,T) = P_{<a}(E \to E') = \frac{\Sigma(E \to E - T)}{\Sigma_{<a}(E)} + \frac{\Sigma(E \to T)}{\Sigma_{<a}(E)}, \tag{24}$$

- *the mean size* of a 'low transferred energy' damage zone

$$R_{<a}(E) = \int_{E_d}^{a} R_P(T)P_a(E,T)\mathrm{d}T, \tag{25}$$

- *the mean distance between two successive collisions* inducing 'low transferred energy' damage zones

$$\lambda_{<a}(E) = \frac{1}{N\Sigma_{<a}(E)}. \tag{26}$$

(c) Overlapping of damage zones

We consider that the distance between two successive damage zones produced by a PKA of energy E as well as the size of these damage zones are given by the mean values $\lambda_a(E)$ and $R_a(E)$, respectively. In the same way, we will use $\lambda_{<a}(E)$ and $R_{<a}(E)$ to characterize the 'low transferred energy' damage zones. '*a*' is the only adjustable parameter of the proposed model and it can be used to select the 'high transferred energy' damage zones which correspond to the sub-cascades (i.e., no overlapping). As an example in iron, Fig. 6(a) and (b) show the evolution of λ_a (E) and $R_a(E)$ as a function of the PKA energy (E) for two values of '*a*' (4 and 13 keV):

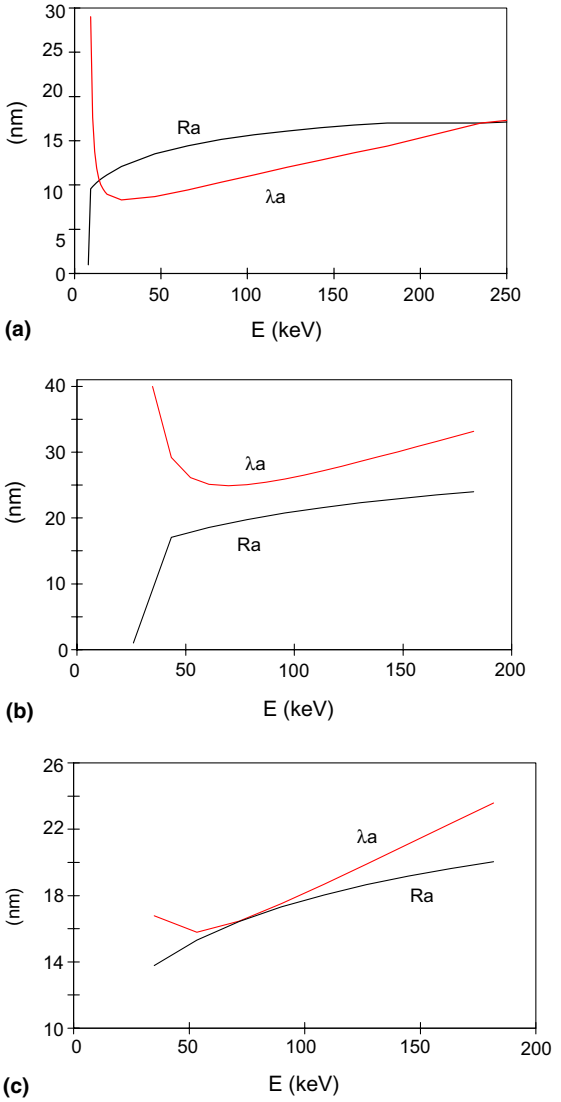

Fig. 6. Evolution of $R_a(E)$ and $\lambda_a(E)$ versus the kinetic energy E of a PKA and as a function of '*a*'. (a) '*a*' = 4 KeV, (b) '*a*' = 13 KeV, (c) '*a*' = 8.3 KeV.

- with '*a*' = 4 keV, the curves have two intersections corresponding to PKA energies of 14 and 230 keV. Between these two energies, there is overlapping of the 'high transferred energy' damage zones which consequently cannot be considered as sub-cascades.
- with '*a*' = 13 keV, λ_a is always higher than $R_a(E)$. The allowed for 'high transferred energy' damage zones may thus be considered as sub-cascades. However, they are rather distant which reveals that smaller sub-cascades are very likely neglected.

In a first approximation, we will consider that the 'high transferred energy' damage zones corresponding to

the sub-cascades are selected when the curves $R_a(E)$ and $\lambda_a(E)$ are tangent. For iron, this leads to 'a' $= a_{\mathrm{sub}} = 8.3$ keV (Fig. 6(c)).

4. Some characteristics of displacement cascades

The size $R_{\mathrm{P}}(T_0)$ of a damage zone and the number of Frenkel pairs $\nu(T_0)$ remaining at the end of its recombination phase strongly depend on the initial kinetic energy T_0 of the SKA: $R_{\mathrm{P}}(T_0)$ and $\nu(T_0)$ may, respectively, vary from few tenths of nanometres and one single Frenkel pair when $T_0 = E_{\mathrm{d}}$ to several hundreds of nanometres and tens of Frenkel pairs for $T_0 = E/2$, with $E = 40$ keV in iron. Hence, according to the initial energy of SKAs, damage zones may have different consequences on the microstructure of irradiated materials. As an example, in reactor pressure vessel steels (e.g., [18,19]), it is now admitted that for high SKA energies the density of residual Frenkel pairs may be locally high enough to induce the formation of germs of point defect clusters and solute-atom/vacancy clusters; whereas for low SKA energies the density of residual Frenkel pairs is locally too low to lead to the formation of germs of solute-atom/vacancy clusters and consequently only germs of point defects clusters are expected. In the REVE approach, we make the distinction between the two cases by supposing that:

- the sub-cascades lead to the formation of germs of both types of defects. This formation is simulated by Molecular Dynamics and Monte Carlo methods;
- the 'low transferred energy' damage zones produced between the sub-cascades lead only to the formation of germs of point defects clusters. The size and numbers of these germs are estimated with laws deduced from statistical analysis of results of displacement cascade simulations, see Section 4.3.

Many characteristics of displacement cascades may be deduced from the model described in Section 3. In this section, we only develop the expressions which are useful to describe the formation of germs of defects, i.e., the mean energy dissipated in sub-cascades, the mean number of sub-cascades and the mean number of residual Frenkel pairs left between the sub-cascades, versus the PKA energy.

4.1. Energy dissipated in sub-cascades

The mean dissipated energies during the slowing-down of a PKA can be determined in the following way:

- for a PKA with an initial energy E_0, we first determine the energy E_1 in a way such that during its slowing-down between E_0 and E_1 the PKA produces one sub-cascade. E_1 can be deduced from the expression

$$\int_{E_1}^{E_0} \frac{\mathrm{d}E}{\left(\frac{\mathrm{d}E}{\mathrm{d}x}\right)_{\mathrm{tot}}} N\Sigma_{a_{\mathrm{sub}}}(E) = 1, \tag{27}$$

- then, we determine the mean energy dissipated in this sub-cascade (recoil energy)

$$\Delta E_{\mathrm{sub}}(E_0, E_1) = N \int_{E_1}^{E_0} \left[\frac{1}{\left(\frac{\mathrm{d}E}{\mathrm{d}x}\right)_{\mathrm{tot}}} \Sigma_{a_{\mathrm{sub}}}(E) \times \int_{a_{\mathrm{sub}}}^{E/2} T P_{a_{\mathrm{sub}}}(E, T)\mathrm{d}T \right] \mathrm{d}E, \tag{28}$$

- as well as the mean energy loss (ΔE_{e}) of the PKA due to electronic interactions

$$\Delta_{\mathrm{e}}(E_0, E_1) = \int_{E_1}^{E_0} \frac{1}{\left(\frac{\mathrm{d}E}{\mathrm{d}x}\right)_{\mathrm{tot}}} \left(\frac{\mathrm{d}E}{\mathrm{d}x}\right)_{\mathrm{e}} \mathrm{d}E, \tag{29}$$

- we also determine the mean energy loss ($\Delta E_{<a_{\mathrm{sub}}}$) of the PKA due to the formation of 'low transferred energy' damage zones

$$\Delta E_{<a_{\mathrm{sub}}}(E_0, E_1) = N \int_{E_1}^{E_0} \left[\frac{1}{\left(\frac{\mathrm{d}E}{\mathrm{d}x}\right)_{\mathrm{tot}}} \Sigma_{<a_{\mathrm{sub}}}(E) \times \int_{E_{\mathrm{d}}}^{a_{\mathrm{sub}}} T P_{<a_{\mathrm{sub}}}(E, T)\mathrm{d}T \right] \mathrm{d}E, \tag{30}$$

or

$$\Delta E_{<a_{\mathrm{sub}}}(E_0, E_1) = N \int_{E_1}^{E_0} \left\{ \frac{1}{\left(\frac{\mathrm{d}E}{\mathrm{d}x}\right)_{\mathrm{tot}}} \times \int_{E_{\mathrm{d}}}^{a_{\mathrm{sub}}} T[\Sigma(E \to E - T) + \Sigma(E \to T)]\mathrm{d}T \right\} \mathrm{d}E, \tag{31}$$

- as well as the mean energy loss $\Delta E_{<E_{\mathrm{d}}}(E_0, E_1)$ of the PKA due to collisions with energy transfers lower than E_{d} (sub-threshold collisions)

$$\Delta E_{<E_{\mathrm{d}}}(E_0, E_1) = N \int_{E_1}^{E_0} \left\{ \frac{1}{\left(\frac{\mathrm{d}E}{\mathrm{d}x}\right)_{\mathrm{tot}}} \int_{0}^{E_{\mathrm{d}}} T[\Sigma(E \to E - T) + \Sigma(E \to T)]\mathrm{d}T \right\} \mathrm{d}E, \tag{32}$$

- the calculated quantities have to verify

$$E_0 - E_1 \approx \Delta E_{\mathrm{sub}}(E_0, E_1) + \Delta E_{\mathrm{e}}(E_0, E_1) + \Delta E_{<a}(E_0, E_1) + \Delta E_{<E_{\mathrm{d}}}(E_0, E_1). \quad (33)$$

The same suite of calculations is then carried out between E_1 and E_2, then between E_2 and E_3 etc, until the PKA has an energy lower than $2a_{\mathrm{sub}}$. Below this value, the PKA cannot produce sub-cascades anymore.

4.2. Number of sub-cascades produced by a PKA

The mean number of sub-cascades produced by a PKA with an initial energy E_0 is given by

- $$N_{\mathrm{sub}}(E_0) = 1 + N \int_{2a_{\mathrm{sub}}}^{E_0} \frac{\Sigma_{a_{\mathrm{sub}}}(E)}{\left(\frac{\mathrm{d}E}{\mathrm{d}x}\right)_{\mathrm{tot}}} \mathrm{d}E, \quad \text{for } 2a_{\mathrm{sub}} \leqslant E_0, \quad (34)$$

the integral in this expression corresponds to the number of sub-cascades induced by the PKA during its slowing-down between E_0 and $2a_{\mathrm{sub}}$; 1 is added to take into account the final damage zone induced by the PKA itself during its slowing-down between $2a_{\mathrm{sub}}$ and E_{d}

- $$N_{\mathrm{sub}}(E_0) = 1, \quad \text{for } a_{\mathrm{sub}} \leqslant E_0 < 2a_{\mathrm{sub}}. \quad (35)$$

In this range of energy, the PKA cannot induce the formation of sub-cascades. However, we count 1 to take the damage zone produced by the PKA itself into account

- $$N_{\mathrm{sub}}(E_0) = 0, \quad \text{for } E_0 < a_{\mathrm{sub}}. \quad (36)$$

SKAs may have a high enough kinetic energy so that the damage zones they induce also split into sub-cascades; the latter have to be taken into account to determine the mean total number of sub-cascades induced in the cascade. Such SKAs must have a kinetic energy higher than $2a_{\mathrm{sub}}$. The total mean number of sub-cascades induced by a PKA is given by

- $$N_{\mathrm{sub}}^{\mathrm{Total}} = N_{\mathrm{sub}}(E_0) + [N_{\mathrm{sub}}(T_1) - 1)] + [N_{\mathrm{sub}}(T_2) - 1] + [N_{\mathrm{sub}}(T_3) - 1] + \cdots \quad (37)$$

where T_1, T_2, etc., are the initial kinetic energies of SKAs (with $T_i \geqslant 2a_{\mathrm{sub}}$) successively induced by the PKA during its slowing-down.

4.3. Number of residual Frenkel pairs left by 'low transferred energy' damage zones

Along its trajectory, a PKA produces 'low transferred energy' damage zones between the sub-cascades. After their recombination phase, each of these zones leaves a number $\nu(T_0)$ of residual Frenkel pairs in the material, where T_0 is the initial energy of the SKA producing the damage zone. The total number $N_{\mathrm{rF}}(E_0)$ of such defects produced by a PKA during its slowing-down from an initial energy E_0 is given by

- $$N_{\mathrm{rF}}(E_0) \approx \int_{2a_{\mathrm{sub}}}^{E_0} \left\{ \frac{1}{\left(\frac{\mathrm{d}E}{\mathrm{d}x}\right)_{\mathrm{tot}}} N\Sigma_{<a_{\mathrm{sub}}}(E) \times \int_{E_{\mathrm{d}}}^{a_{\mathrm{sub}}} \nu(T) P_{<a_{\mathrm{sub}}}(E, T) \mathrm{d}T \right\} \mathrm{d}E, \quad \text{for } 2a_{\mathrm{sub}} \leqslant E_0. \quad (38)$$

This expression ignores the residual point defects left during the slowing-down of the PKA from $2a_{\mathrm{sub}}$ to E_{d}. Indeed, these defects are formed in the final damage zone produced by the PKA which is counted as a 'high transferred energy' damage zone [see expression (34)]

- $$N_{\mathrm{rF}}(E_0) = 0, \quad \text{for } a_{\mathrm{sub}} \leqslant E_0 < 2a_{\mathrm{sub}}. \quad (39)$$

In this range of initial energy, the damage zone produced by the PKA is counted as a sub-cascade [see expressions (35)]; this is why there is no 'low transferred energy' damage zone

- $$N_{\mathrm{rF}}(E_0) = \nu(E_0), \quad \text{for } E_0 < a_{\mathrm{sub}}. \quad (40)$$

In this range of initial energy, the PKA can only induce a 'low transferred energy' damage zone.

For iron, several expressions have been proposed for $\nu(E)$ (e.g., [20,21]) from Molecular Dynamics simulations; in INCAS, we used [21]

$$\nu(E) = 5E^{0.74} \quad (\text{for } E \leqslant 20 \text{ keV}). \quad (41)$$

In this expression, E is the damage energy (keV) dissipated in nuclear collisions (= recoil energy−energy losses in electronic interactions). However, since the PKAs or SKAs concerned by this expression have a low kinetic energy ($\leqslant a_{\mathrm{sub}}$), we neglect their electronic interactions and consider that their initial kinetic energy (recoil energy) equals the damage energy.

As already mentioned, SKAs may have a kinetic energy high enough ($T_0 \geqslant 2a_{\mathrm{sub}}$) to lead to the fact that the damage zones they induce also split into sub-cascades; the 'low transferred energy' damage zones formed between them also have to be taken into account. Hence, the mean total number of residual Frenkel pairs left by a PKA between the sub-cascades it has induced is given by

$$N_{\mathrm{rF}}^{\mathrm{Total}} = N_{\mathrm{rF}}(E_0) + N_{\mathrm{rF}}(T_1) + N_{\mathrm{rF}}(T_2) + N_{\mathrm{rF}}(T_3) + \cdots \quad (42)$$

where T_1, T_2, etc., are the initial kinetic energies of SKAs (with $T_i \geqslant 2a_{\mathrm{sub}}$) successively induced by the PKA during its slowing-down. The residual point defects may be isolated or clustered in small germs. Their distribution depends on the irradiated materials. For example, for iron, statistical analyses of results of

Table 1
Parameters describing displacement cascades (iron self-irradiation, $a_{sub} = 8.3$ keV)

PKA initial energy (keV)	Number of sub-cascades	PKA energy range $E_{i+1} - E_i$ (keV)	Energy dissipated in sub-cascades ΔE_{sub} (keV)	Electronic losses ΔE_e (keV)	Losses in LTE[a] $\Delta E_{<a}$ (keV)	Losses in sub-threshold collisions $\Delta E_{<E_d}$ (keV)	Total dissipated energy[b]/ $(E_{i+1} - E_i)$ (keV)
(Part A)							
3000	23	3000–2382[c]	27	PKA:546	PKA:16	PKA:0.8	620/618
			12	SKA:6	SKA:12	SKA:0.2	
		2382–1912[c]	25	PKA:402	PKA:15	PKA:0.7	473/470
			12	SKA:6	SKA:12	SKA:0.2	
		1912–1544[c]	23	PKA:302	PKA:15	PKA:0.6	370/368
			11	SKA:6	SKA:12	SKA:0.2	
		1544–1250[c]	21	PKA:229	PKA:14	PKA:0.6	295/294
			11	SKA:6	SKA:12	SKA:0.2	
		1250–1012[c]	20	PKA:176	PKA:13	PKA:0.5	239/238
			10	SKA:6	SKA:13	SKA:0.2	
		1012–818[c]	18	PKA:135	PKA:13	PKA:0.5	196/194
			9	SKA:6	SKA:14	SKA:0.2	
		818–657	44	104	12	0.4	160/161
		657–523	42	80	12	0.4	134/134
		523–412	39	61	11	0.4	111/111
		412–318	37	46	11	0.3	94/94
		318–240	33	34	10	0.3	77/78
		240–176	30	25	10	0.3	65/64
		176–122	26	18	10	0.2	54/54
		122–78	21	12	10	0.2	43/44
		78–44	16	8	10	0.2	34/34
		44–0	44	–	–	–	44/44
(Part B)							
2000	20	2000–1613[c]	24	PKA:320	PKA:15	PKA:0.7	389/387
			11	SKA:6	SKA:12	SKA:0.2	
		1613–1306[c]	22	PKA:243	PKA:14	PKA:0.6	310/307
			11	SKA:6	SKA:13	SKA:0.2	
		1306–1058[c]	20	PKA:186	PKA:13	PKA:0.5	249/248
			10	SKA:6	SKA:13	SKA:0.2	
		1058–855[c]	18	PKA:143	PKA:13	PKA:0.5	204/203
			9	SKA:6	SKA:14	SKA:0.2	
		855–688[c]	16	PKA:110	PKA:12	PKA:0.4	167/167
			8	SKA:6	SKA:14	SKA:0.2	
		688–549	42	85	12	0.4	139/139
		549–433	40	64	11	0.4	115/116
		433–337	37	48	11	0.3	96/96
		337–256	34	36	11	0.3	81/81
		256–188	31	27	10	0.3	68/68
		188–132	29	19	10	0.2	58/56
		132–87	22	13	10	0.2	45/45
		87–50	17	9	10	0.2	36/37
		50–21	10	6	12	0.2	28/29
		21–0	21	–	–	–	21/21
(Part C)							
1000	14	1000–808[c]	18	PKA:134	PKA:13	PKA:0.5	195/192
			9	SKA:6	SKA:14	SKA:0.2	
		808–649	44	103	12	0.4	159/159
		649–516	42	79	12	0.4	133/133
		516–406	39	60	11	0.4	110/110
		406–314	36	45	11	0.3	92/92
		314–236	33	33	10	0.3	76/78

(*continued on next page*)

Table 1 (*continued*)

PKA initial energy (keV)	Number of sub-cascades	PKA energy range $E_{i+1} - E_i$ (keV)	Energy dissipated in sub-cascades ΔE_{sub} (keV)	Electronic losses ΔE_e (keV)	Losses in LTE[a] $\Delta E_{<a}$ (keV)	Losses in sub-threshold collisions $\Delta E_{<E_d}$ (keV)	Total dissipated energy[b]/ $(E_{i+1} - E_i)$ (keV)
		236–172	30	24	10	0.3	64/64
		172–119	26	17	10	0.2	53/53
		119–76	21	12	10	0.2	43/43
		76–42	16	8	10	0.2	34/34
		42–0	42	–	–	–	42/42
500	8	500–392	39	58	11	0.3	108/108
		392–302	36	43	11	0.3	90/90
		302–227	33	32	10	0.3	75/75
		227 164	29	23	10	0.3	62/63
		164–113	25	16	10	0.2	51/51
		113–71	20	11	10	0.2	41/42
		71–38	15	8	11	0.2	34/33
		38–0	38	–	–	–	38/38
(Part D)							
200	5	200–142	28	20	10	0.2	58/58
		142–95	23	14	10	0.2	47/47
		95–57	18	10	10	0.2	38/38
		57–26	12	6	12	0.2	30/31
		26–0	26	–	–	–	26/26
100	3	100–61	19	10	10	0.2	39/39
		61–30	13	7	11	0.2	31/31
		30–0	30	–	–	–	30/30

[a] LTE: low transferred energy.
[b] Total dissipated energy $= (\Delta E_{sub} + \Delta E_e + E_{<a} + \Delta E_{<E_d})_{PKA} + (\Delta E_{sub} + \Delta E_e + \Delta E_{<a} + \Delta E_{<E_d})_{SKA}$.
[c] Range of PKA energy where the SKA has enough energy to produce 2 sub-cascades.

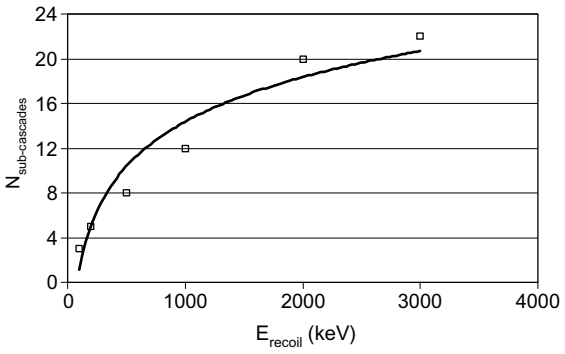

Fig. 7. Number of sub-cascades created in iron versus the PKA recoil energy: simulation results (symbols) and associated trend curve.

displacements cascades simulated by Molecular Dynamics [9,22–24] show that in iron most of the residual vacancies are isolated. They also show [21,24] that the distribution of the residual self interstitial atoms can be roughly estimated as follows: 60% are isolated, 20% are in clusters of size 2, 10% in clusters of size 3, 6% in clusters of size 4, 3% in clusters of size 5 and 11% in clusters of size 6.

5. Applications

A computer code was written in Fortran 77 to solve all the INCAS equations presented in the previous sections. As an example of application, this code was used to describe displacement cascades induced in pure elements: firstly iron, then aluminium, copper, niobium, silver, indium, barium, lanthanum and gold. Most of these elements have no special link with irradiation effects in LWRs, they were selected to make comparisons with other studies or to assess the effect on the results of the atomic number, atomic mass or atomic density. The following PKA recoil energies were allowed for: 3, 2, 1, 0.5, 0.2, 0.1, 0.3 MeV. Finally, as a first application concerning neutron irradiation effects in LWR materials, the INCAS code was used to determine the sub-cascade spectrum induced in iron by the neutron spectrum corresponding to the central channel of the High Flux Irradiation Reactor (HFIR) of Oak Ridge National Laboratory.

Table 2
Some physical characteristics and a_{sub} values for aluminium, iron copper, niobium, silver, indium, barium, lanthanum and gold

	Al	Fe	Cu	Nb	Ag	In	Ba	La	Au
Atomic number	13	26	29	41	47	49	56	57	79
Atomic mass	27	56	63	93	108	115	137	139	197
Atomic density (10^{28} cm^{-3})	6	8.5	9.8	5.56	5.9	3.82	1.57	1.33	5.9
Crystallographic structure	fcc	bcc	fcc	bcc	fcc	tetra	bcc	hcp	fcc
a_{sub} (keV)	1.3	8	9.8	22.1	31	34.2	46	48.7	105

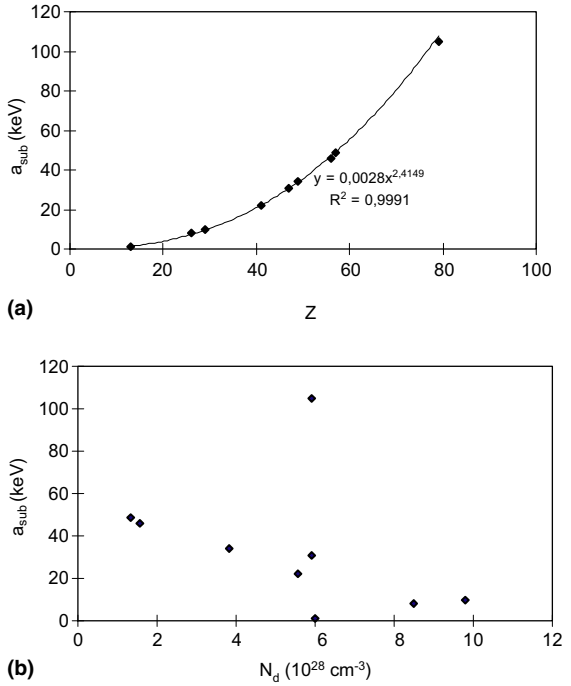

Fig. 8. Evolution of a_{sub} versus: (a) the atomic number Z and (b) the atomic density N_d of the irradiated element.

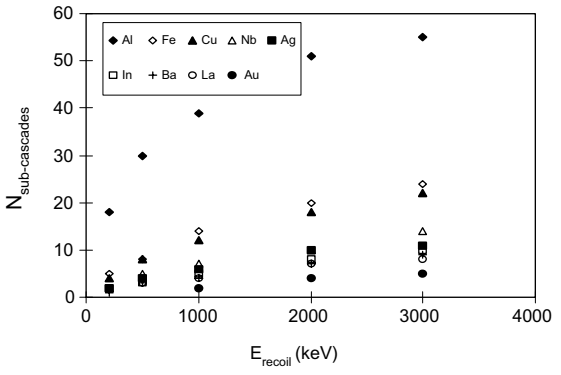

Fig. 9. Number of sub-cascades created in aluminium, copper, niobium, silver, indium, barium, lanthanum and gold versus the PKA recoil energy.

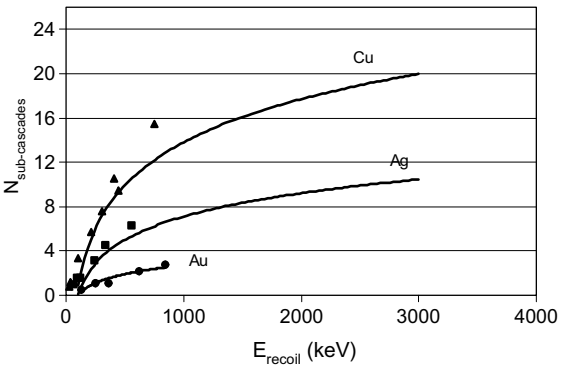

Fig. 10. Number of sub-cascades created in copper, silver an gold versus the PKA recoil energy. Curve: INCAS simulation; symbols: Marlowe simulation [6].

5.1. Cascades in pure elements

5.1.1. Iron

To describe displacement cascades in iron, we used $a_{sub} = 8.3$ keV as determined in Section 3.2(c). Table 1 gives the results obtained by following the series of calculation described in Section 4. When SKAs produce sub-cascades, their energy losses in electronic interactions, 'low transferred energy' damage zones and sub-threshold collisions between the sub-cascades can be calculated as those of the PKA. These SKA energy losses are also given in Table 1. It can be noticed that:

- SKAs produce sub-cascades when the PKA recoil energy ranges between 500 and 3000 keV;
- the mean energy dissipated in sub-cascades ranges between 8 and 44 keV;
- as already noticed by Sigmund [17], the mean energy dissipated in 'low energy transferred' damage zones between two sub-cascades is of the order of a_{sub};
- the mean energy losses in sub-threshold collisions ($T < E_d$) is always negligible;
- the total dissipated energies (last column) are in conformity with the energy losses of the PKA ($E_{i+1} - E_i$).

The mean number of sub-cascades is plotted versus the PKA recoil energy in Fig. 7. It can be noticed that the curve trends towards an asymptote as the PKA energy increases. This effect results from the increase of the electronic interactions which become predominant for kinetic energies higher than about 1 MeV (see Fig. 2).

5.2. Effect of the irradiated element

As for iron, INCAS was used to describe cascades in aluminium, copper, niobium, silver, indium, barium, lanthanum and gold. Some characteristics of these elements are given in Table 2. The corresponding a_{sub} values are also given in Table 2 and plotted versus the atomic number and atomic density on Fig. 8. It appears that a_{sub} increases steadily with the atomic number (Fig. 8(a)), but is not directly correlated with the atomic density (Fig. 8(b)). The evolution of the mean number of sub-cascades versus the PKA recoil energy is given in Fig. 9. For a same PKA recoil energy, the mean number of sub-cascades increases as the atomic number decreases. This trend is in conformity with other studies (e.g., [5,6,25]). Concerning Al, Cu, Ag, Au, the results obtained with INCAS can be quantitatively compared with those obtained by Heinisch and Singh with the Marlowe code [6]. These authors developed a computational method to objectively identify sub-cascades simulated with Marlowe and thus have probably produced the most reliable results on this topic up to now. The evolutions of the mean number of sub-cascades, versus the PKA recoil energy, obtained from both methods are compared in Fig. 10; the results are very similar.

5.3. HFIR sub-cascade spectrum

In the REVE project, a first tool aimed at simulating irradiation effects in reactor pressure vessel steel is under development. This tool, called RPV-1, is described in a comprehensive way in [26]. It relies on three modules which can be shortly presented as follows:

- a '*short-term irradiation*' module treats the neutron spectrum to provide the PKA spectrum (with the code SPECMIN [4] [27,28]). Then, using this spectrum as source term, INCAS gives the induced sub-cascade spectrum (number of sub-cascades versus their dissipated energy). By convoluting the sub-cascade spectrum and the distribution of germs of hardening defects produced by each sub-cascade (given in a database called CASCADE), the module defines the source term of a long-term irradiation module.
- a '*long-term irradiation*' module mainly includes a Rate Theory code (called MF-VISC) to simulate the evolution of the irradiated microstructure from about 10^{-3} s to years.
- a '*hardening*' module finalizes the simulation by simulating a tensile test with a mesoscopic code (a Foreman and Makin-type code called DUPAIR),

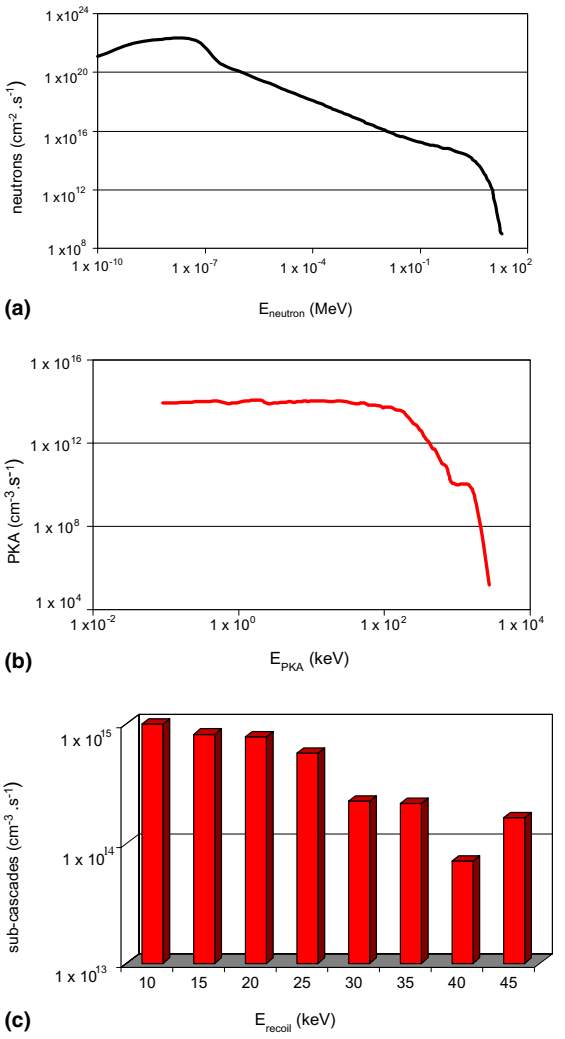

Fig. 11. Neutron spectrum corresponding to the central channel of HFIR as well as the induced PKA and sub-cascade spectra in iron.

[4] SPECMIN is a simplified version of the code SPECTER; both codes have been developed by L. Greenwood from Pacific Northwest National Laboratory. SPECMIN provides less information than SPECTER, but allows the simulations to be operated on a PC-type computer where its typical running time is about few seconds. It is written in FORTRAN.

using a database of pinning forces (called DEFECT).

As an example of use of INCAS in the short-term module, Fig. 11 shows the neutron spectrum corresponding to the central channel of the HFIR reactor as well as the induced PKA and sub-cascade spectra in iron.

6. Conclusion

The REVE (REactor for Virtual Experiments) is an international project aimed at developing tools to simulate neutron radiation effects in LWR materials. One of the important steps of the project is to describe the displacement cascades induced by neutrons. Accordingly, the Department of Material Studies of Electricité de France developed an analytical model based on the binary collision approximation. This model, called INCAS (INtegration of CAScades), was devised to be applied on pure elements; however, it can also be used on diluted alloys (reactor pressure vessel steels, etc.) or alloys composed of atoms with similar masses (stainless steels, etc.).

INCAS enables in particular to determine the mean number of sub-cascades induced by a PKA (depending on its energy) as well as the mean energy dissipated in each of them. The mean PKA energy dissipated in electronic interactions and sub-threshold collisions (collisions with lattice-atoms in which the transferred energy is lower than the displacement energy) are also available. In addition, INCAS gives the mean number of Frenkel pairs produced between the sub-cascades. It was not possible to carry out an experimental validation of INCAS. However, it was noticed that its results are in conformity with those obtained from other approaches. Finally, as first application, INCAS was applied to determine the sub-cascade spectrum induced in iron by the neutron spectrum corresponding to the central channel of HIFR.

A computer code was written in Fortran 77 to solve all the equations of INCAS. It can be used through a friendly interface and with the help of a user guide. This code is available on request.

Acknowledgements

We express our gratefulness to Professor A.I. Ryazanov (Kurchatov Institute) who helped us start this work, Professor P. Sigmund (Odense University) who developed most of the ideas used to devise INCAS more than 30 years ago and who patiently initiated us into the formalism required for the treatment of the interactions between particles, and Professor R. Odette (University of California Santa Barbara) for his kind hosting and fruitful discussions on the REVE project.

References

[1] S. Jumel, C. Domain, J. Ruste, J.C. van Duysen, C. Becquart, A. Legris, P. Pareige, A. Barbu, E. van Walle, R. Chaouadi, M. Hou, G.R. Odette, R. Stoller, B.D. Wirth, J. Test. Eval. 30 (2002) 37.
[2] S. Jumel, RPV-1: a virtual reactor to simulate irradiation effect in pressurized water reactor pressure vessel steels, PhD thesis, Université de Lille, 2004.
[3] M.T. Robinson, I.M. Torrens, Phy. Rev. B 9 (1974) 5008.
[4] P.S. Ziegler, J.P. Biersack, U. Littmark, The Stopping and Range of Ions in Solids, Pergamon, New-York, 1985, p. 48.
[5] Y. Satoh, S. Kojina, T. Yoshiie, M. Kiriani, J. Nucl. Mater. 179–181 (1991) 901.
[6] H. Heinisch, B.N. Singh, Philos. Mag. A 67 (2) (1993) 407.
[7] ASTM E521, Standard practice for neutron radiation damage simulation by charged particle irradiation, Annual Book of ASTM Standards, vol. 12.02.
[8] C. Lehmann, in: S. Amelinckx, R. Gevers, J. Nihoul (Eds.), Defects in Crystalline Solids, 10, Elsevier, North-Holland, 1977.
[9] R.E. Stoller, L.R. Greenwood, J. Nucl. Mater. 271&272 (1999) 57.
[10] R.E. Stoller, A.F. Calder, Statistical analysis of a library of molecular dynamics cascade simulations in iron at 100 K, Ninth International Conference on Fusion Reactor Materials, Colorado Springs, CO, 10–15 October 1999, J. Nucl. Mater. 283–287 (2000) 746.
[11] M.T. Robinson, J. Nucl. Mater. 216 (1994) 1.
[12] J. Lindhard, V. Nielsen, M. Scharff, Det Kongelige Danske Videnskaberbernes Selskab Matematisk-fysiske Meddelelser 36, 10, 1968.
[13] K.B. Winterbon, P. Sigmund, J.B. Sanders, Mat. Fys. Medd. Dan. Vid. Selsk. 37 (14) (1970) 1.
[14] Bohr, N., Mat. Fys Medd. Dan. Vid. Selsk. 18(40.8) (1948) 1.
[15] K.B. Winterbon, Radiat. Eff. 13 (1972) 215.
[16] H. Bethe, F. Zeits, Physik 76 (1932) 293.
[17] P. Sigmund, G.P. Scheidler, G. Roth, Spatial distribution of defects in cascades. Black spot defects in electron irradiated copper, BNL report–50083 (C-52) 1968.
[18] P. Auger, P. Pareige, M. Akamatsu, J.C. van Duysen, J. Nucl. Mater. 211 (1994) 194.
[19] M. Akamatsu, J.C. van Duysen, P. Pareige, P. Auger, J. Nucl. Mater. 225 (1995) 192.
[20] D.J. Bacon, A.F. Calder, F. Gao, V.G. Kapinos, S. Wooding, Nucl. Instrum. and Meth. B 102 (1995) 49.
[21] C.S. Becquart, C. Domain, J.C. van Duysen, J.M. Raulot, J. Nucl. Mater. 294 (2001) 274.
[22] W.J. Phythian, R.E. Stoller, A.J.E. Foreman, A.F. Calder, D.J. Bacon, J. Nucl. Mater. 223 (1995) 245.

[23] R.E. Stoller, G.R. Odette, B.D. Wirth, J. Nucl. Mater. 251 (1997) 49.
[24] C. Domain, private communication.
[25] Y. Satoh, T. Yoshiie, M. Kiriani, J. Nucl. Mater. 191–194 (1992) 1101.
[26] S. Jumel, J.C. van Duysen, RPV-1: a virtual test reactor to simulate irradiation effects in light water reactor pressure vessel steels, J. Nucl. Mater. (submitted for publication).
[27] L. Greenwood, J. Nucl. Mater. 216 (1994) 29.
[28] R.E. Stoller, L.R. Greenwood, An evaluation of through-thickness changes in primary damage production in commercial reactor pressure vessels, 20th International Symposium on the Effects of Radiation on Materials, Williamsburg, VA, 6–8 June 2000, American Society of Testing and Materials in ASTM STP 1405, p. 204.